

# Inverse Design of Tightly Woven Smart Fabrics

Einav Berin<sup>1</sup> and Hillel Aharoni<sup>1</sup>

<sup>1</sup>Department of Complex Systems, Weizmann Institute of Science, Rehovot  
7610001, Israel

## Abstract

We present a geometric framework for the inverse design of smart woven fabrics composed of non-uniformly shrinking threads. A sufficiently tight weaving structure imposes strong local criteria on the material deformation and reduces the local geometry to a single scalar degree of freedom. Control over this degree of freedom can be achieved through simple calibration for each specific material system, via either mechanical experiments or numerical simulations. This reduction allows us to inverse-design a woven smart fabric, that conforms to an arbitrary target geometry when actuated, by solving a nonlinear hyperbolic partial differential equation. We validate this approach by deriving the thread-level actuation required for specific target geometries. We present both exact analytic solutions for symmetric shapes and a numerical optimization method for arbitrary freeform surfaces. These results confirm the practicality of our framework in achieving programmable, complex three-dimensional shaping.

## Introduction

Fabrics are everywhere. They are lightweight, durable, scalable, and versatile materials, used in a wide variety of technologies, applications, and everyday uses since ancient times. They are composed of yarns or threads interlaced into a two-dimensional periodic structure. The threads are held together by the topological constraints of the interlacing, which depend on the specific interlacing process, such as weaving, knitting, crocheting, and others. Several strategies have been developed for modeling fabrics, including yarn-path tracking [1], mass–spring and finite-element models [2, 3], and continuum formulations that approximate the fabric as a two-dimensional surface [4, 5]. Some fabrics are made loose, attributing them with flexibility and the ability to stretch and shear. Others are made tight, typically by introducing tension during manufacturing, endowing them with a more robust geometry [6].

Extensive efforts have been invested in recent decades to develop smart materials that undergo controlled deformations in response to external stimuli [7]. Examples include hydrogels [8], nematic elastomers [9], shape-memory polymers [10], and more. Recent advances in 3D printing have enabled the fabrication of smart threads that can be actuated by temperature [11], light, or electric fields [12]. Using such threads enables the manufacturing of woven, knitted, and embroidered smart fabrics [13, 14, 15].

Programmable surfaces made of smart materials are used in soft robotics [16], biomedicine [17], 4D printing [18], and the fashion industry [19]. A central challenge in studying such surfaces is understanding the relationship between local actuation and global shape. This can be framed as two complementary problems. The forward problem asks, given the local material response at every point, what global shape will a surface assume upon actuation? The inverse problem seeks the local material response that needs to be programmed into the material at every point to achieve a desired target global shape. These problems have been studied in various systems, including two-dimensional liquid crystal elastomer sheets [20], auxetic materials [19], responsive gel sheets [21], deployable origami [22], and others.

In this work, we focus on a system of a tightly woven smart fabric composed of threads with non-uniform shrinkage profiles, as shown in Fig. 1. We focus on geometric constraints and do not consider dynamics or friction. We demonstrate that the tight weave structure confines the range of local deformations to a single curve, which can be calibrated according to the working material. Constructing an orthogonal coordinate system based on the tight-weaving structure reveals a simple relation between the remaining controllable

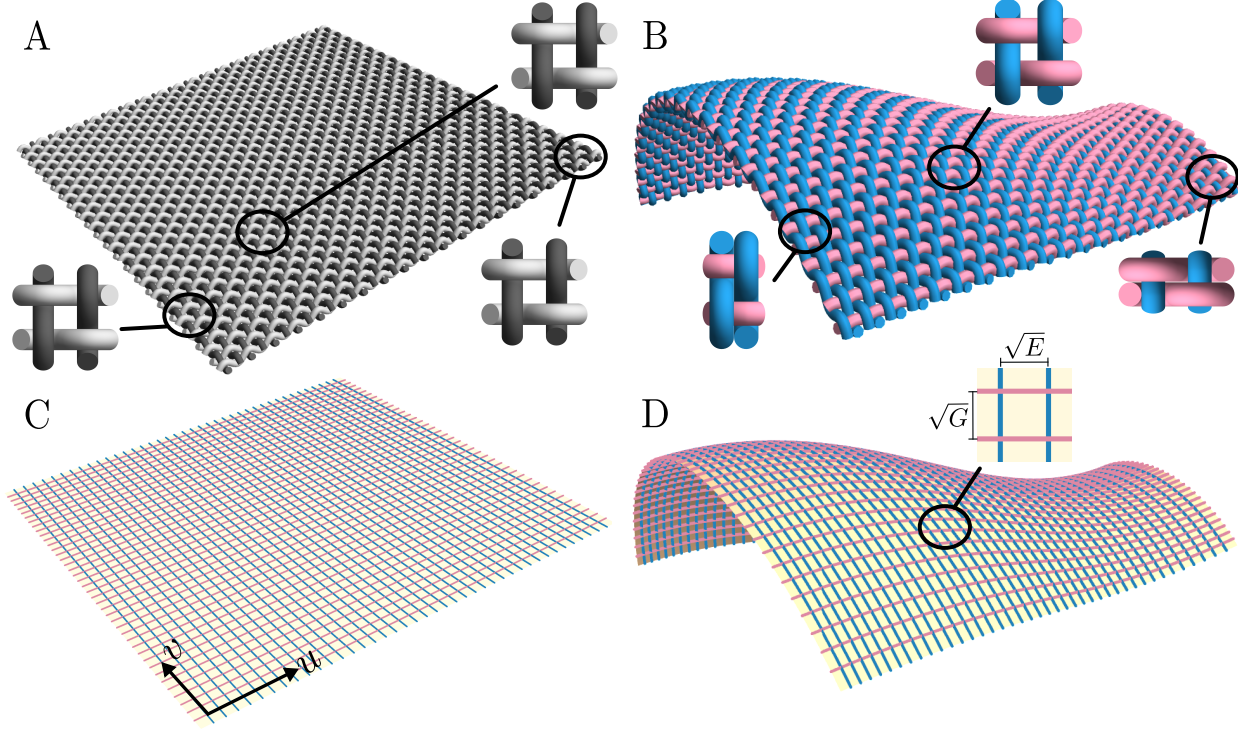


Figure 1: Illustration of a plain woven smart fabric. (A) A pre-actuated smart fabric. The fabric is flat and uniform (as shown by the identical zoomed-in unit cells). (B) When actuated, the spatially varying pre-programmed thread response deforms each unit cell differently, endowing the fabric with a non-Euclidean geometry that invokes its morphing into a non-planar surface. (C) Material coordinates  $(u, v)$  aligned with warp and weft threads, respectively, are used to keep track of the fabric's geometry and shape. (D) The local tangent spacings of adjacent warp/weft threads define the metric scale factors  $\sqrt{E}$  and  $\sqrt{G}$ . In a tightly woven fabric, shear is suppressed, and threads remain orthogonal.

local degree of freedom and the actuated surface geometry. We utilize this approach to address both the forward and inverse design problems, producing explicit recipes for creating smart fabrics that deform into arbitrary desired shapes.

## Results

A plain woven fabric is a textile structure formed by the interlacing of warp and weft threads, where each weft thread passes over and under successive warp threads in an alternating sequence. We describe the configuration of a large-scale woven fabric as a two-dimensional (2D) surface representing the mid-plane of the structure, coarse-grained at the scale of the weaving unit cell. We use coordinates  $u$  and  $v$  that follow the woven threads; namely,  $u$  counts the warp threads and  $v$  the weft threads, measured from some arbitrary origin. We assume that the weaving unit-cell is much smaller than system-size or spatial gradients in the composition of the smart fabric, and thus describe the shape of the fabric in terms of a continuous function  $\mathbf{f}(u, v) \in \mathbb{R}^3$ . The two-dimensional geometry of the fabric at a given state is captured in the metric tensor [23]

$$ds^2 = E(u, v) du^2 + 2F(u, v) dudv + G(u, v) dv^2, \quad (1)$$

which captures the lateral dimensions of each unit cell in the weave structure.

In the general case, the metric components  $E, F, G$  may vary across the fabric and change when the fabric is deformed (either by external forcing or by actuation of the smart threads). In a tightly-woven fabric, however, threads lose their local freedom to change position or angle and the fabric becomes rigid and stiff. Experiments show that increasing thread density rigidifies both bending and shear [24, 25] and

diminishes the maximal shear angle [26]. Since the symmetry of the weaving unit-cell favors neither shear direction, and because we assume that lateral gradients at the scale of the unit cell are small,  $F = 0$  is imposed. The same jamming transition also imposes a nontrivial relationship between  $E$  and  $G$  in the tight limit due to the weaving topology. Intuitively, adjacent warp threads cannot be too close to each other as weft threads must be allowed to pass between them, and vice versa. The exact relationship depends on the physical properties of the threads and the interaction between them.

In a smart fabric, threads change (typically reduce) their rest length upon actuation. The degree of local compression is assumed to be a controllable degree of freedom in the manufacturing process, e.g., the cross-linking density at each point along a liquid crystal elastomer thread. In a wide regime of fabric parameters (discussed in the following), this actuation brings the smart fabric into the tight-weaving regime by inducing jamming and thus rigidifying the local fabric geometry as discussed above.

To illustrate this, we simulate the mechanical response of a plain woven fabric using a three-dimensional finite element model. The model focuses on a single unit cell of the weave, with periodic boundary conditions imposed. Each thread is represented as a chain of springs, arranged according to the interlacing topology of a plain woven fabric. The elastic energy consists of a stretching term that penalizes deviation from the springs' rest lengths, and a bending term that penalizes angles between neighboring springs. The ratio between the bending and stretching moduli determines an "effective thickness", which depends on the physical nature of the threads and their elastic anisotropy. In addition, the threads have a finite physical thickness, which prevents them from approaching each other closely beyond their diameter. We thus introduce a hard-cylinder repulsive term to the elastic energy, which strongly penalizes inter-thread distance smaller than 1 (which sets the units for all the other length scales in the problem).

We simulate two physical models. The first model includes bending, representing threads made from an isotropic elastic material, such that the effective thickness is identical to the physical thickness. The second model includes negligible bending (still needed for regularization), representing threads made of bundled stiff fibers [27, 28] (effective thickness  $\ll$  physical thickness). In the vanishing-bending limit, we expect this model to produce the *ropelength-critical weave* (following [29]), namely the woven structure of least arclength constrained to an inter-thread distance of 1. We conjecture that the ropelength-critical weave has an explicit analytical formula as piecewise planar-circular arcs and critical clasps; see Sec. A.1 for more details. Here we do not prove this; instead, we obtain it numerically via constrained optimization (Appendix Sec. A.1).

For each physical model, we minimize the total energy of the unit cell for a given set of rest lengths of the threads to determine the optimal rest configuration of the fabric. In particular, we retrieve the projected lengths of the threads, which translate to  $2\sqrt{E}$  and  $2\sqrt{G}$  in our chosen coordinate system. The results corresponding to simulations at different rest lengths of the threads are plotted in Fig. 2.

As Fig. 2 shows, the tight weaving regime comprises a large domain of thread rest-lengths that, when woven, reach the jamming transition. The metric components of such fabrics indeed collapse to a one-dimensional curve, namely a strict equality relating  $E$  and  $G$ . Thus, one can write the metric Eq. 1 in the form

$$ds^2 = E(\alpha(u, v)) du^2 + G(\alpha(u, v)) dv^2, \quad (2)$$

where  $E$  and  $G$  are known functions that are determined by the threads' physical attributes. The scalar function  $\alpha(u, v)$  depends on the local rest lengths of the threads at each unit cell, and determines the point on the universal  $E - G$  curve that is reached in equilibrium.

A relatively simple relation that makes a good approximation for the two models we've simulated, and many other physical thread structures, reads

$$\sqrt{E} = 2 \cos^c \alpha, \quad \sqrt{G} = 2 \sin^c \alpha, \quad \text{where } \alpha \in \left(0, \frac{\pi}{2}\right). \quad (3)$$

If one assumes that the threads are laterally incompressible, then  $\alpha$  is further restricted such that  $E, G \geq 1$ . In each model, we fit  $c$ . We find good agreement at  $c = 0.52 \pm 0.01$  for the finite-bending model and  $c = 0.50 \pm 0.01$  for the negligible-bending model. In the numerical examples that follow, we use Eq. 3 with  $c = 0.52$  to demonstrate our findings.

Gauss's Theorema Egregium connects the metric tensor and the Gaussian curvature of a surface  $K(u, v)$  [23]. The Gaussian curvature associated with Eq. 2 is

$$K(u, v) = \frac{(EG)' (\alpha_v^2 E' + \alpha_u^2 G') - 2GE (\alpha_v^2 E'' + \alpha_u^2 G'' + \alpha_{uu} G' + \alpha_{vv} E')}{4E^2 G^2}. \quad (4)$$

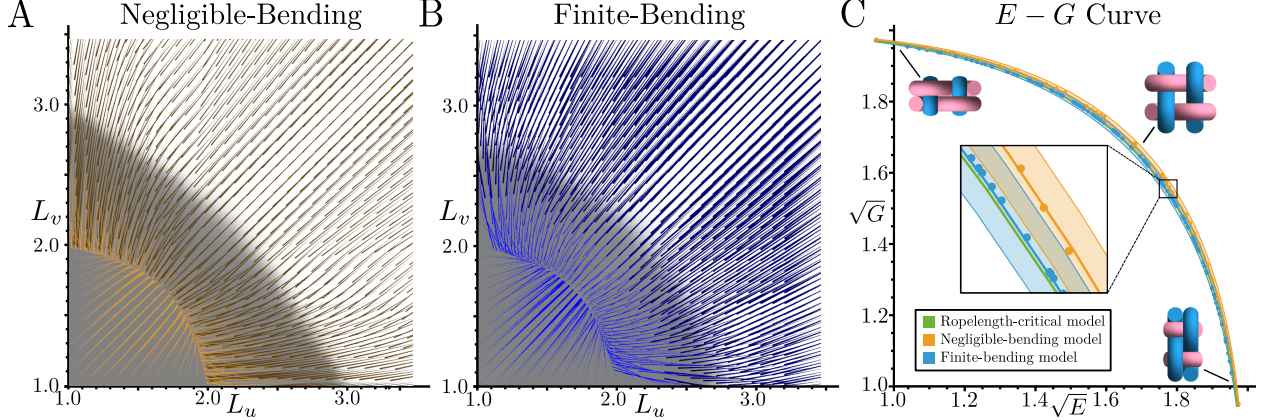


Figure 2: Energy-minimizing configurations of a plain-weave unit cell for various prescribed thread rest lengths, for two physical thread models: (A) negligible bending modulus (orange), and (B) bending modulus of an elastic rod (blue). Each tapered line starts (narrow end) at the prescribed target lengths  $(L_u, L_v)$ , and ends (wide end) at the tangentially projected equilibrium lengths of the final configuration, namely the metric components  $(\sqrt{E}, \sqrt{G})$ , respectively (all lengths are measured in units of the thread diameter). As seen in (A,B), an extended domain within the space of thread rest lengths (marked in gray) collapses onto a one-dimensional curve of unit-cell equilibrium metrics. (C) The tight-weave  $E - G$  curves obtained for the two physical models in (A) and (B), fitted to the one-parameter form  $\sqrt{E} = 2 \cos^c \alpha$ ,  $\sqrt{G} = 2 \sin^c \alpha$  ( $R^2 = 99.5\%$ ,  $99.86\%$ , respectively). The fitted parameters are  $c = 0.52 \pm 0.01$  and  $c = 0.50 \pm 0.01$ , respectively. Also shown is the E-G curve of the ropelength-critical weave, obtained numerically by constrained optimization. As expected, it lies close to the negligible-bending curve.

This expression readily describes the geometry of an actuated, tightly woven fabric in terms of its local structure field  $\alpha(u, v)$ . It thus allows predicting the resulting surface shape, solving the forward design problem. Namely, from the thread actuation profile, manifested in  $\alpha(u, v)$  via a calibration curve of the type of Fig. 2, we calculate the (rigid) intrinsic geometry of the actuated fabric.

We turn to study the inverse design problem. Eq. 4 can be rewritten as a second-order PDE for  $\alpha(u, v)$

$$G' \alpha_{uu} + E' \alpha_{vv} = \frac{(EG)'}{2EG} (\alpha_v^2 E' + \alpha_u^2 G') - \alpha_v^2 E'' - \alpha_u^2 G'' - 2EGK(u, v). \quad (5)$$

In some special cases Eq. 5 is analytically solvable, for example, the case of  $E = \cos^2 \alpha$ ,  $G = \sin^2 \alpha$  and  $K(u, v) = \text{const}$  in which Eq. 5 becomes the Sine-Gordon equation. Such solutions are not likely to be useful since  $E(\alpha)$  and  $G(\alpha)$  are typically calibrated experimentally, and  $K(u, v)$  represents an arbitrary target surface. In some cases, additional symmetries allow for significantly simplifying Eq. 5. This is the case for target surfaces of revolution, where we assume that the thread structure shares the same symmetry, namely that threads lie along latitudes and longitudes of the surface. The inverse design problem reduces to a second-order ODE,

$$\alpha''(u) + A[\alpha] \alpha'(u)^2 = B[\alpha] K \left( \int \sqrt{E(\alpha(u))} du \right), \quad (6)$$

where  $A[\alpha] = \frac{d}{d\alpha} \log \left( \frac{G'}{\sqrt{EG}} \right)$  and  $B[\alpha] = -\frac{2EG}{G'}$ . Given initial conditions for  $\alpha(u)$ , Eq. 6 can be solved, either analytically (see Sec. A.4) or numerically. In Fig. 3 we solve Eq. 6 for several surfaces of revolution.

Nonetheless, the general case makes a well-posed hyperbolic problem. The effect of the volume excluded by each thread on the trajectories of crossing threads implies that  $dE/dG < 0$ . Without loss of generality, we choose  $E(\alpha)$  to be a monotonically decreasing function, and  $G(\alpha)$  a monotonically increasing function. Thus, Eq. 5 is a hyperbolic PDE on  $\alpha(u, v)$  with characteristic curves that are transverse to both families of threads. Of course, the PDE depends on the value of the target Gaussian curvature at each point. To complete a well-posed Cauchy initial-value problem, the hyperbolic PDE requires a Cauchy-type initial condition [30]. Thus, the problem is fully set given the following: (i) a target surface, (ii) a curve on the target surface, and

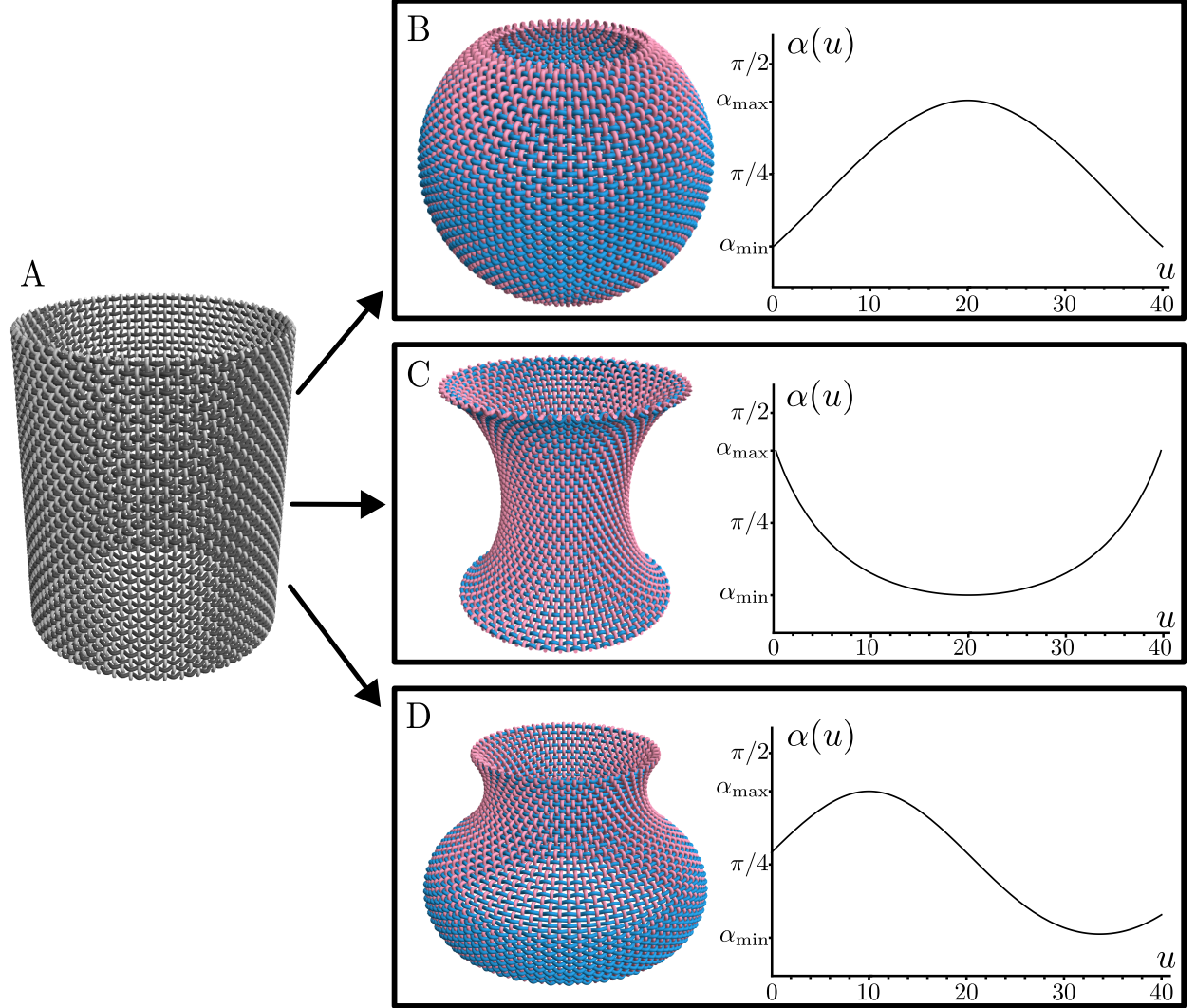


Figure 3: Inverse design of woven smart-fabric surfaces of revolution. (A) A pre-actuated woven cylinder. (B-D) Actuating the smart fabric with different actuation profiles  $\alpha(u)$  deforms the cylinder into (B) a sphere, (C) a pseudo-sphere, and (D) a vase-shaped surface of revolution. The actuation profile required to obtain each desired shape was solved using [Eq. 6](#).

(iii) a shrinkage profile along the curve. The chosen curve is destined to be the actuated shape of one of the threads,  $v = 0$ . The profile  $\alpha(u, 0)$  along the curve and the curve's geodesic curvature completely determine the perpendicular derivative  $\partial_v \alpha(u, 0)$  (see Appendix [Sec. A.3](#)), and thus complete the setting of a Cauchy problem. This guarantees a unique solution for  $\alpha(u, v)$  in the surroundings of the initial curve, which may extend all the way to the boundaries or diverge at some finite horizon [\[30\]](#).

The solution to a Cauchy problem, as stated above, is a solution to the inverse design problem of smart fabrics. Given a target surface, we obtain an explicit function  $\alpha(u, v)$ , which can then be transcribed to the explicit shrinkage of each thread at each point using [Eq. 5](#). Therefore, given a robust and precise technique for the manufacturing of smart fabrics with given thread-shrinkage profiles, we provide an explicit recipe for fabrics that will deform into an arbitrary target geometry upon actuation, at least locally.

For practical implementations of the inverse problem, the target surface will be given in a discrete form, such as a triangular mesh. An algorithm for numerically solving the initial value problem described above on such a mesh is presented in [Sec. A.3](#), in the form of pseudo-code. Such a solution is not guaranteed to extend to the full mesh. An alternative approach is to search for a global coordinate parameterization of the

target surface, in which the metric of the surface at any point takes the form Eq. 2 for given functions  $E$  and  $G$ . Since a global solution is not guaranteed, the idea is to find a parametrization that best approximates the local rules. Finding surface parametrizations that approximate different local relations is an active field of study in computer graphics and geometric processing. Many methods were developed to address similar problems, such as the local/global approach [31], the commuting vector fields approach [32], and more.

Recently, a numerical approach that is very natural to our problem was presented by Corman and Crane [33]. The approach is designed to find rectangular surface parameterizations, namely those with  $F = 0$ . The method establishes integrability conditions for an orthogonal local frame field to represent a coordinate-derived frame. Their algorithm then searches for an optimal parameterization with respect to these conditions and any additional energy term written in terms of the local frame. For our purposes, we simply construct an energy penalty for deviating from the target metric Eq. 3. This requires an adaptation of the code used in [33] (see Sec. A.5). Approximate solutions to the inverse design problem are shown in Fig. 4.

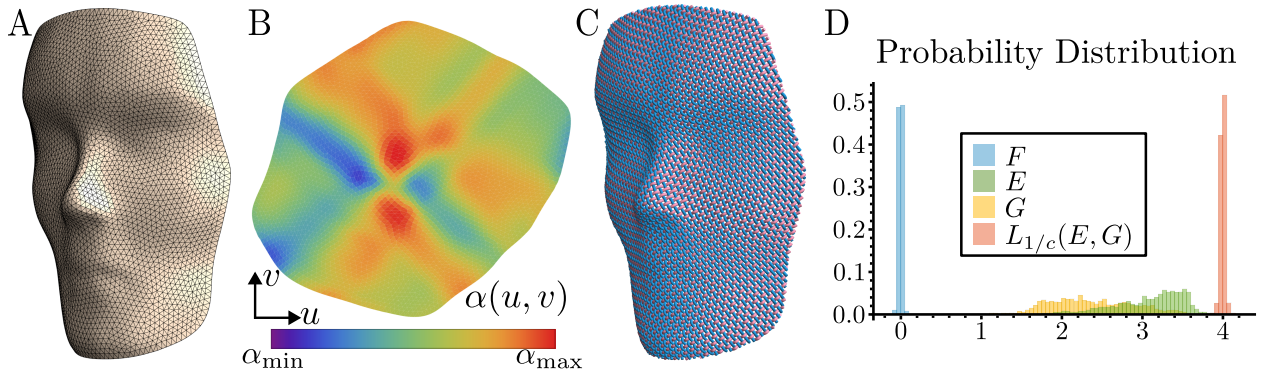


Figure 4: Inverse design of a generic woven smart-fabric surface. (A) Target face geometry given as a triangular mesh. (B) An approximate solution of Eq. 3 obtained numerically using the adapted Corman-Crane algorithm (Sec. A.5). The algorithm outputs both the weaving domain and the actuation parameter  $\alpha(u, v)$  at each point, needed for manufacturing the smart fabric. (C) Upon actuation, the initially planar fabric will adopt the geometry of the target face shape, with the shown thread pattern. (D) Histogram of metric elements confirming the numerical solution. The sharp distribution of the  $F$  component at 0 confirms orthogonality, while the sharp distribution of the  $(1/c)$ -norm of  $(E, G)$  at 4 confirms adherence to the imposed tight-weave  $E - G$  curve Eq. 3.

In this example, the target surface is a face represented as a triangular mesh. The Corman–Crane method produces a rectangular parameterization consistent with the tight-weaving constraints, to which threads can be aligned (Fig. 4). The actuation parameter  $\alpha$  varies across the surface, evident from the differing eccentricity of the rectangular patches in the chin region compared to the nose. This variation is also visualized in the parameterization domain, where each face is colored by its  $\alpha$  value (Fig. 4C). The histogram of the metric components on each face, (Fig. 4D), confirms that the parametrization is orthogonal and satisfies the constraint  $E + G \equiv 1$ . Together, these results demonstrate that the discrete construction provides a faithful, though approximate, realization of the target geometry.

## Discussion

In this work, we establish a geometric framework for the inverse design of tightly woven smart fabrics. In the tight-weaving regime, the mechanical jamming of threads imposes an orthogonal coordinate system with strictly coupled metric components. Through finite element simulations of weaving unit cells, we validate that this coupling follows a universal master curve. For a range of physical models, this curve can be very well approximated by Eq. 3 with some value of the parameter  $c$ . Based on this constitutive relation, we formulate the inverse design problem as a hyperbolic partial differential equation for the local actuation field  $\alpha(u, v)$ . We provide constructive solutions for this system, ranging from an exact analytical solution for

surfaces of revolution to a global optimization method for general discrete surfaces.

Practical realizations of active woven textiles have recently been demonstrated by Silva et al., who successfully integrated liquid crystal elastomer (LCE) filaments into standard weaving patterns [13]. Their approach used a hybrid structure in which one set of threads (the weft) is active and exhibits a uniform shrinkage profile upon heating, while the orthogonal set (the warp) remains passive. A particularly relevant case is their polar weave design, which is fabricated as a flat disk and transforms into a cone, effectively forming a positive curvature singularity at the tip. While the threads remain orthogonal, the radial divergence of the passive warp threads implies that the inter-thread spacing increases linearly with the distance from the tip. Consequently, such a structure cannot comply with the tight-weaving condition described in our model on an extended domain. A polar weaving system could still be described by our model (Sec. A.2) if radial threads are constantly added during weaving away from the center to maintain the tight structure.

Although we considered the simple case of plain woven fabrics, our assumptions also hold for more complex fabrics in the tight regime. The majority of textile structures possess a symmetry that excludes spontaneous shear, and the jamming transition is expected to eliminate an additional degree of freedom. The calibration curve Fig. 2 for such fabrics may be more complicated and harder to model. Nonetheless, once it is achieved (if only by experimental measurement), our suggested inverse design protocols may be readily implemented.

Nonetheless, implementing our model for knitted and other fabrics may require addressing an additional component. The weaving structure preserves coarse-grained symmetry with respect to normal reflections and thus prefers no extrinsic curvature; Conversely, knitted fabrics exhibit a preferred non-zero saddle-like extrinsic curvature that stems from the knitting structure [34], and is responsible for the fabric’s tendency to strongly curl at its boundaries [35]. Utilizing this phenomenon grants the manufacturer access not only to the fabric’s intrinsic geometry but also, to some degree, to its extrinsic curvatures. This, in turn, may allow control over the resulting shape choice among all isometries of the target surface [20].

Contrary to local solutions to the inverse problem, global solutions do not always exist. Nonetheless, as shown in several similar problems [32], global solutions are expected to exist if they are allowed to contain point disclinations, around which the warp and weft threads switch roles to create a 90-degree surplus/deficit angle. We are not aware of a weaving mechanism that allows for introducing such objects into a woven fabric; however, if such a mechanism exists, global inverse design is readily feasible with our numerical inverse design scheme.

## Acknowledgments

We thank Etienne Corman and Keenan Crane for clarifications and advice on adapting their code. We thank Myfanwy E. Evans and Randall D. Kamien for fruitful discussions. This research was supported by the Israel Science Foundation (grant No. 2677/20).

## References

- [1] Tianyong Zheng, Jing Wei, Zhengtao Shi, Tingting Li, and Zhen Wu. An overview of modeling yarn’s 3d geometric configuration. *Journal of Textile Science and Technology*, 1(1):12–24, 2015.
- [2] Xavier Provot. Deformation constraints in a mass-spring model to describe rigid cloth behavior. In *Proceedings of Graphics Interface*, 1995.
- [3] David Baraff and Andrew Witkin. Large steps in cloth simulation. In *SIGGRAPH ’98: Proceedings of the 25th Annual Conference on Computer Graphics and Interactive Techniques*, 1998.
- [4] J. R. Womersley. 6.—the application of differential geometry to the study of the deformation of cloth under stress. *Journal of the Textile Institute Transactions*, 28(3):T97–T113, 1937.
- [5] Samuel Poincloux, Mokhtar Adda-Bedia, and Frédéric Lechenault. Geometry and elasticity of a knitted fabric. *Phys. Rev. X*, 8:021075, 2018.

- [6] Philippe Boisse, Nabil Hamila, Elizabeth Guzman-Maldonado, Angela Madeo, Guillaume Hivet, and Francesco dell'Isola. The bias-extension test for the analysis of in-plane shear properties of textile composite reinforcements and prepgs: a review. *International Journal of Material Forming*, 10:473–492, 2017.
- [7] Hyun Kim, Suk-kyun Ahn, D. Mackie, Jinhyeong Kwon, Shi-Hyeong Kim, Changsoon Choi, Y. Moon, Ha Beom Lee, and S. Ko. Shape morphing smart 3d actuator materials for micro soft robot. *Materials Today*, 41:243–269, 2020.
- [8] Yoshitsugu Hirokawa and Toyoichi Tanaka. Volume phase transition in a nonionic gel. *The Journal of chemical physics*, 81(12):6379–6380, 1984.
- [9] Jürgen Küpfer and Heino Finkelmann. Nematic liquid single crystal elastomers. *Die Makromolekulare Chemie, Rapid Communications*, 12(12):717–726, 1991.
- [10] Andreas Lendlein, Annette M Schmidt, and Robert Langer. Ab-polymer networks based on oligo ( $\varepsilon$ -caprolactone) segments showing shape-memory properties. *Proceedings of the National Academy of Sciences*, 98(3):842–847, 2001.
- [11] Arda Kotikian, Ryan L Truby, John William Boley, Timothy J White, and Jennifer A Lewis. 3d printing of liquid crystal elastomeric actuators with spatially programed nematic order. *Advanced materials*, 30(10):1706164, 2018.
- [12] Jiaqi Liu, Yuchong Gao, Haihuan Wang, Ryan Poling-Skutvik, Chinedum O. Osuji, and Shu Yang. Shaping and locomotion of soft robots using filament actuators made from liquid crystal elastomer–carbon nanotube composites. *Advanced Intelligent Systems*, 2(6):1900163, 2020.
- [13] Pedro E. S. Silva, Xueyan Lin, Maija Vaara, Mithila Mohan, Jaana Vapaavuori, and Eugene M. Terentjev. Active textile fabrics from weaving liquid crystalline elastomer filaments. *Advanced materials (Weinheim)*, 35(14):e2210689–n/a, 2023.
- [14] Jiahao Sun, Wei Liao, and Zhongqiang Yang. Additive manufacturing of liquid crystal elastomer actuators based on knitting technology. *Advanced materials (Weinheim)*, 35(36):e2302706–e2302706, 2023.
- [15] Antonio Proctor Martinez, Alicia Ng, So Hee Nah, and Shu Yang. Active-textile yarns and embroidery enabled by wet-spun liquid crystalline elastomer filaments. *Advanced Functional Materials*, page 2400742.
- [16] Robert F. Shepherd, Filip Ilievski, Wonjae Choi, Stephen A. Morin, Adam A. Stokes, Aaron D. Mazzeo, Xin Chen, Michael Wang, and George M. Whitesides. Multigait soft robot. *Proceedings of the National Academy of Sciences*, 108(51):20400–20403, 2011.
- [17] Gregory P Crawford, Scott J Woltman, and Gregory D Jay. Liquid-crystal materials find a new order in biomedical applications. *Nature materials*, 6(12):929–938, 2007.
- [18] A. Sydney Gladman, Elisabetta A. Matsumoto, Ralph G. Nuzzo, L. Mahadevan, and Jennifer A. Lewis. Biomimetic 4d printing. *Nature Materials*, 15(4):413–418, 4 2016.
- [19] Mina Konaković, Keenan Crane, Bailin Deng, Sofien Bouaziz, Daniel Piker, and Mark Pauly. Beyond developable: computational design and fabrication with auxetic materials. *ACM transactions on graphics*, 35(4):1–11, 2016.
- [20] Hillel Aharoni, Yu Xia, Xinyue Zhang, Randall D. Kamien, and Shu Yang. Universal inverse design of surfaces with thin nematic elastomer sheets. *Proceedings of the National Academy of Sciences*, 115(28):7206–7211, 2018.
- [21] Jungwook Kim, James A. Hanna, Myunghwan Byun, Christian D. Santangelo, and Ryan C. Hayward. Designing responsive buckled surfaces by halftone gel lithography. *Science (American Association for the Advancement of Science)*, 335(6073):1201–1205, 2012.

[22] Xiangxin Dang, Fan Feng, Paul Plucinsky, Richard D. James, Huiling Duan, and Jianxiang Wang. Inverse design of deployable origami structures that approximate a general surface. *International Journal of Solids and Structures*, 234-235:111224, 2022.

[23] Manfredo P do Carmo. *Differential Geometry of Curves and Surfaces: Revised and Updated Second Edition*. Dover Publications, New York, 2016.

[24] Md Samsu Alam, Abhijit Majumdar, Anindya Ghosh, et al. Role of fibre, yarn and fabric parameters on bending and shear behaviour of plain woven fabrics. *Indian Journal of Fibre & Textile Research (IJFTR)*, 44(1):9–15, 2019.

[25] Jinlian. Hu and England) Textile Institute (Manchester. *Structure and mechanics of woven fabrics*. Woodhead Pub., Cambridge, 2004.

[26] John Skelton. Fundamentals of fabric shear. *Textile Research Journal*, 46(12):862–869, 1976.

[27] F. Barsi, B. Carboni, and W. Lacarbonara. A new mechanical model of short wire ropes: Theory and experimental validation. *Engineering structures*, 323:119217–, 2025.

[28] Mohammed Adnan, Robert A Pinnick, Zhao Tang, Lauren W Taylor, Sushma Sri Pamulapati, Gianni Royer Carfagni, and Matteo Pasquali. Bending behavior of cnt fibers and their scaling laws. *Soft matter*, 14(41):8284–8292, 2018.

[29] Jason Cantarella, Joseph H G Fu, Rob Kusner, John M Sullivan, and Nancy C Wrinkle. Criticality for the gehring link problem. *Geometry & topology*, 10(4):2055–2115, 2006.

[30] Yehuda Pinchover and Jacob Rubinstein. *An Introduction to Partial Differential Equations*. Cambridge University Press, New York, 1 edition, 2005.

[31] Ligang Liu, Lei Zhang, Yin Xu, Craig Gotsman, and Steven J. Gortler. A local/global approach to mesh parameterization. *Computer graphics forum*, 27(5):1495–1504, 2008.

[32] Andrew O. Sageman-Furnas, Albert Chern, Mirela Ben-Chen, and Amir Vaxman. Chebyshev nets from commuting polyvector fields. *ACM Trans. Graph.*, 38(6), November 2019.

[33] Etienne Corman and Keenan Crane. Rectangular surface parameterization. *ACM Trans. Graph.*, 44(4), 2025. Code available at <https://github.com/etcorman/RectangularSurfaceParameterization>, accessed: 2025-07-21.

[34] Lauren Niu, Genevieve Dion, and Randall D. Kamien. Geometric modeling of knitted fabrics. *Proceedings of the National Academy of Sciences - PNAS*, 122(7):e2416536122–, 2025.

[35] Arif Kurbak and Ozgur Ekmen. Basic studies for modeling complex weft knitted fabric structures part i: A geometrical model for widthwise curlings of plain knitted fabrics. *Textile Research Journal*, 78(3):198–208, 2008.

[36] Code available at <https://doi.org/10.5281/zenodo.18324284>.

[37] John M Sullivan and Nancy C Wrinkle. Some ropelength-critical clasps. 2004.

## A Supporting Information

Appendix	Content Description
A.1	The ropelength problem and the clasp configuration.
A.2	Formulas for Gaussian curvature $K$ in Cartesian and polar coordinates.
A.3	Geometric construction of the solution for the Cauchy problem
A.4	Analytical solutions of the inverse design ODE for surfaces of revolution and constant curvature.
A.5	Adaptation of Corman-Crane method for tight-weave metric constraints.

Table 1: List of Appendices and Contents

Code File	Content Description
constrained_optimization.py	Numerical optimization Python code
woven_fabric_optimization.jl	Energy minimization Julia code

Table 2: List of code files available in [36]

### A.1 The Ropelength Problem

Ropelength problems seek the configuration of a knot or link that minimizes its total arc length while maintaining a unit-thickness constraint [29]. The *clasp* problem is a simple nontrivial instance of this problem. It consists of two arcs whose endpoints are constrained to lie on prescribed planes, with the unit-distance constraint on their closest approach. While a standard clasp is symmetric, a generalized clasp allows the endpoints to lie on planes inclined at different angles [37]. The explicit configurations for different critical clasp curves are given by elliptic integrals. These curves exhibit two characteristic features: a region of very large curvature near the center of each rope, and a small gap between the two rope components at their centers.

Guided by this picture, we identify the tightly woven fabric unit cell as a critical ropelength problem, with the weaving topology and periodic boundary conditions. We address this problem using numerical optimization with a hard minimal-distance constraint between two orthogonal families of curves. We employ the *Sequential Least Squares Programming (SLSQP)* algorithm, which iteratively approximates the arclength objective function and the distance constraints as a quadratic program, allowing the system to converge to the jamming transition where the threads are in a state of minimal length subject to the constraint. We find that the optimal curves decompose into regular circular arcs and segments of generalized clasp solutions. This is analogous to the ropelength-critical solution for the Borromean rings, which similarly comprises piecewise analytic segments rather than a single smooth curve, as discussed in [29].

### A.2 Gaussian Curvature Formulae

Gauss's *Theorema Egregium* states that the Gaussian curvature  $K$  of a two-dimensional surface is an intrinsic invariant that can be computed directly from the metric tensor and its derivatives.

Given a general two-dimensional metric

$$ds^2 = E(u, v) du^2 + 2F(u, v) du dv + G(u, v) dv^2,$$

the Gaussian curvature is given by the Brioschi formula:

$$K = \frac{-1}{2\sqrt{EG - F^2}} \left[ \frac{\partial}{\partial u} \left( \frac{G_u - 2F_v + E_v}{\sqrt{EG - F^2}} \right) + \frac{\partial}{\partial v} \left( \frac{E_v - 2F_u + G_u}{\sqrt{EG - F^2}} \right) \right].$$

As we discuss in the manuscript, the general metric describing the geometry of a tight fabric is

$$ds^2 = E(\alpha(u, v)) du^2 + G(\alpha(u, v)) dv^2.$$

The Gaussian curvature is then

$$K(u, v) = \frac{(EG' + E'G)(\alpha_v^2 E' + \alpha_u^2 G') - 2GE(\alpha_v^2 E'' + \alpha_u^2 G'' + \alpha_{uu}G' + \alpha_{vv}E')}{4E^2 G^2}.$$

The metric tensor that describes polar weaving is, in polar coordinates:

$$ds^2 = E(\alpha(r, \theta)) dr^2 + r^2 G(\alpha(r, \theta)) d\theta^2.$$

The Gaussian curvature is then

$$K(r, \theta) = \frac{(EG' + E'G)(\alpha_\theta^2 E' + r^2 \alpha_r^2 G') - 2GE(\alpha_\theta^2 E'' + \alpha_r^2 r^2 G'' + \alpha_{rr}r^2 G' + \alpha_{\theta\theta}E' + 2\alpha_r r G')}{4r^2 E^2 G^2} + \frac{\alpha_r E' (2G + rG')}{4r G E^2}.$$

### A.3 Geometric construction of a local solution for the Cauchy problem

The inverse design problem for a tight smart fabric whose local deformation obeys the metric

$$ds^2 = E(\alpha(u, v)) du^2 + G(\alpha(u, v)) dv^2, \quad (\text{A.1})$$

can be written as a hyperbolic PDE

$$G' \alpha_{uu} + E' \alpha_{vv} = \frac{(EG)'}{2EG} (\alpha_v^2 E' + \alpha_u^2 G') - \alpha_v^2 E'' - \alpha_u^2 G'' - 2EGK(u, v). \quad (\text{A.2})$$

The associated Cauchy problem requires, in addition to [Eq. A.2](#), also the value of  $\alpha(u, 0)$  and  $\alpha_v(u, 0)$  on an initial curve  $v = 0$  (transverse to the characteristic curves).  $\alpha_v(u, 0)$  can be calculated from  $\alpha(u, 0)$  and the geodesic curvature of the initial curve  $\kappa_g(u)$  via the relation [\[23\]](#)

$$\alpha_v(u, 0) = -\frac{2\kappa_g(u) E(\alpha(u, 0)) \sqrt{G(\alpha(u, 0))}}{E'(\alpha(u, 0))}. \quad (\text{A.3})$$

Geometrically, the solution is constructed as follows: we start with an arbitrary curve on the target surface, which we identify with the  $u$ -curve  $v = 0$ . We arbitrarily choose  $\alpha(u, 0)$ , which in turn defines scale marks along the initial curve, separated by the distance  $\sqrt{E(\alpha(u, 0))}$ . From each mark, we emit a  $v$ -curve, perpendicular to the initial curve, at speed  $\sqrt{G(\alpha(u, 0))}$ . The loci along these  $v$ -curves after an infinitesimal time  $\epsilon$  make the  $u$ -curve  $v = \epsilon$ . Iterating this construction produces a local rectangular coordinate system on the surface, which obeys the metric tensor [Eq. A.1](#). The procedure breaks down when two such  $u$ -curves intersect (namely  $E(\alpha) = 0$ ) or when two  $v$ -curves intersect ( $G(\alpha) = 0$ ). The geometric construction is summarized in [Alg. 1](#).

### A.4 Inverse Problem Symmetric Solution

In the symmetric case of a surface of revolution, [Eq. 6](#) reads

$$\alpha''(u) + A[\alpha(u)] \alpha'(u)^2 = B[\alpha(u)] K(s(u)), \quad s(u) = \int_0^u \sqrt{E(\alpha(\tilde{u}))} d\tilde{u}, \quad (\text{A.4})$$

with

$$A[\alpha] = \frac{d}{d\alpha} \log \left( \frac{G'(\alpha)}{\sqrt{E(\alpha)G(\alpha)}} \right), \quad B[\alpha] = -\frac{2E(\alpha)G(\alpha)}{G'(\alpha)}.$$

Define

$$w(u) := \alpha'(u) \frac{G'(\alpha(u))}{\sqrt{E(\alpha(u))G(\alpha(u))}}. \quad (\text{A.5})$$

---

**Algorithm 1** Geometric Construction of a Local Solution to the Cauchy Problem

---

1: **Input:**

- Target surface,
- Initial curve  $\gamma_0$  on the surface,
- Initial profile  $\alpha(u, 0)$  along  $\gamma_0$ .

2: **Output:** Surface parameterization  $(u, v)$  and structure field  $\alpha(u, v)$ , in which the metric of the target surface reads Eq. A.1.

3: Parametrize the curve  $\gamma_0(u)$  such that  $\gamma'_0(u) = \sqrt{E(\alpha(u, 0))}$ .

4: Set  $v \leftarrow 0$ .

5: Set positive  $\delta v \ll$  surface dimensions and curvature scales.

6: **while**  $\forall u: E(\alpha(u, v)) > 0$  and  $G(\alpha(u, v)) > 0$  **do**

7:   **for** all  $u$  **do**

8:      $\gamma_{v+\delta v}(u) = \exp_{\gamma_v(u)} \left( \sqrt{G(\alpha(u, v))} \delta v \cdot \widehat{\gamma'_v(u)^\perp} \right)$     (where  $\exp$  is the exponential map)

9:   **end for**

10:   Set  $\alpha(u, v + \delta v) = E^{-1}(\gamma'_{v+\delta v}(u)^2)$ .

11:   Set  $v \leftarrow v + \delta v$ .

12: **end while**

---

Then Eq. (A.4) is equivalent to the first-order system

$$\begin{aligned} \alpha'(u) &= w(u) \frac{\sqrt{E(\alpha(u))} G(\alpha(u))}{G'(\alpha(u))}, \\ s'(u) &= \sqrt{E(\alpha(u))}, \\ w'(u) &= -2\sqrt{E(\alpha(u))} G(\alpha(u)) K(s(u)), \end{aligned} \tag{A.6}$$

with initial data

$$\alpha(0) = \alpha_0, \quad s(0) = s_0, \quad w(0) = w_0 = \alpha'(0) \frac{G'(\alpha_0)}{\sqrt{E(\alpha_0) G(\alpha_0)}}.$$

For the special case of constant Gaussian curvature  $K(s) \equiv K_0$ , the system (A.6) admits a first integral

$$w(\alpha)^2 + 4K_0 G(\alpha) = C, \tag{A.7}$$

so that  $\alpha(u)$  is given implicitly by the integral

$$u - u_0 = \pm \int_{\alpha_0}^{\alpha(u)} \frac{G'(\tilde{\alpha})}{\sqrt{E(\tilde{\alpha})} G(\tilde{\alpha}) (C - 4K_0 G(\tilde{\alpha}))} d\tilde{\alpha}, \tag{A.8}$$

with the constant  $C$  fixed by the initial slope  $\alpha'(0)$  via (A.7).

## A.5 Rectangular Parametrization Algorithm

To generate global parameterizations on discrete triangular meshes (as shown in Fig. 4), we utilized the *Rectangular Surface Parameterization* framework developed by Cormen and Crane [33]. Their algorithm optimizes for an orthogonal coordinate system aligned with a target frame field.

We adapted their open-source implementation to enforce the specific geometric constraints of tightly woven fabrics. The original objective function minimizes standard distortion metrics (e.g., conformality or area distortion). We replaced this energy term in the file `objective_ortho_param.m` with a penalty that enforces the specific coupling between the metric components  $E$  and  $G$  derived from our physical model:

$$E^c + G^c = \text{Constant} \tag{A.9}$$

The modification involves calculating the error potential `err_diag` and its associated Jacobian derivatives to guide the optimizer toward the tight-weave solution. The MATLAB implementation of this specific constraint is as follows:

```
% Enforce physical constraint: E^c + G^c = 2
err_diag = log(exp(-2*c*ut*integral_tri - 2*c*vt*integral_tri)/2 + ...
               exp(-2*c*ut*integral_tri + 2*c*vt*integral_tri)/2);

% Jacobian calculations for the optimizer
da = -2*c*ones(Src.nf,1)/3;
db = (2*c/3)*(exp(4*c*vt*integral_tri) - 1)./(exp(4*c*vt*integral_tri) + 1);
daa = zeros(Src.nf,1);
dab = zeros(Src.nf,1);
dbb = (16*(c^2)/9)*exp(4*vt*c*integral_tri)./(exp(4*vt*c*integral_tri) + 1).^2;
```